Advanced Ceramics Progress: Vol. 10, No. 2, (Spring 2024) 9-16

Materials and Energy Research Center
MERC

Contents lists available at ACERP

Advanced Ceramics Progress

Journal Homepage: www.acerp.ir

Original Research Article

Effect of pH of the Electroless Bath on Microstructure and Corrosion Behavior of Ni-Co-La_2O_3-CeO_2 Coating

Katayoon Soleimani Roodi [a], Hadi Ebrahimifar [b,*], Farhad Mohsenifar [c]

[a] *MSc Candidate, Department of Materials Engineering and Metallurgy, Faculty of Engineering, Shahid Bahonar University, of Kerman, Kerman, Iran.*

[b] *Associate Professor, Department of Materials Engineering, Faculty of Mechanical and Materials Engineering, Graduate University of Advanced Technology, Kerman, Iran.*

[c] *Assistant Professor, Mechanical Engineering Department, Faculty of Engineering, Higher Education Complex of Bam, Bam, Kerman, Iran.*

* Corresponding Author Email: H.ebrahimifar@kgut.ac.ir (H. Ebrahimifar) URL: https://www.acerp.ir/article_209453.html

ARTICLE INFO

Article History:
Received: 14 September 2024
Revised: 09 October 2024
Accepted: 12 November 2024

Keywords:
Corrosion Resistance,
Composite Coating,
Potentiodynamic Polarization,
Electrochemical Impedance Spectroscopy

ABSTRACT

In this study, Ni-Co-La_2O_3-CeO_2 composite coatings were deposited on an AISI 430 steel substrate using the electroless method. The microstructure and corrosion behavior of coatings obtained at different bath pHs (8, 8.5, 9, 9.5, and 10) were investigated. Coating characterization was performed using a scanning electron microscope (SEM). To assess corrosion resistance, potentiodynamic polarization and electrochemical impedance spectroscopy (EIS) tests were conducted in a 3.5% NaCl aqueous solution. Microstructural examination showed that the coating formed at pH 9 has greater uniformity than the other coatings. Additionally, under this condition, the highest weight percentage of reactive elements (La and Ce) was present in the coating. The Tafel polarization test results demonstrated that applying the composite coating significantly reduces the corrosion current density of the uncoated sample. The positive effect of the coating on increasing the corrosion resistance of the steel is particularly significant for the coating formed at pH 9. In this case, the corrosion current density was reduced by more than 20 times (from 17.35 $\mu A \cdot cm^{-2}$ to 0.8 $\mu A \cdot cm^{-2}$) compared to the uncoated sample. The results obtained from electrochemical impedance spectroscopy (EIS) further support these findings. According to the EIS data, the charge transfer resistance for the uncoated sample was 4089 $\Omega \cdot cm^2$, while applying coatings at pH levels of 8, 8.5, 9, 9.5, and 10 increased the charge transfer resistance to 13,214, 19,840, 28,318, 17,060, and 9446 $\Omega \cdot cm^2$, respectively.

https://doi.org/10.30501/acp.2024.478445.1163

1. INTRODUCTION

430 stainless steel, containing 16-18% chromium, has a relatively low carbon content (0.12% C) and a ferritic matrix (Mosavi & Ebrahimifar, 2020). Chromium is the most important alloying element that protects stainless steels from oxidation and corrosion. The oxidation and corrosion resistance of these steels increases with higher chromium content (Yu et al., 2018).

Due to high nickel prices, there is a trend to switch from austenitic to ferritic stainless steels; however, ferritic stainless steels offer weaker mechanical and corrosion resistance properties compared to austenitic stainless steels because of their relatively weaker ferritic matrix, which somewhat limits their applications. Surface modification and deposition of a protective film or coating on these steels can expand their desirable properties and, consequently, their range of applications (Amin et al., 2016; Chen et al., 2022).

Composite coatings containing nickel and cobalt are among the most widely used coatings (Elkhoshkhany et al., 2017). Electroless and electroplating are two common methods for applying these coatings on metal surfaces.

Please cite this article as: Soleimani Roodi, K., Ebrahimifar, H. & Mohsenifar, F. (2024). Effect of pH of the Electroless Bath on Microstructure and Corrosion Behavior of Ni-Co-La2O3-CeO2 Coating, *Advanced Ceramics Progress*, 10(2), 9-16. https://doi.org/10.30501/acp.2024.478445.1163

Electroless technology, invented in 1946, is a chemical deposition method in which there is no external current, and the required electrons are provided by a chemical reaction in the solution (Kumar et al., 2020; Pancrecious et al., 2018). Electroless nickel coatings have a wide range of industrial applications due to their unique properties, such as excellent adhesion to the substrate, uniform thickness, high hardness, and wear resistance. Additionally, they exhibit higher hardness, wear, and corrosion resistance than those obtained by electroplating, though they are more brittle (Chintada et al., 2021; Fayomi et al., 2019). Nickel coatings alone have low corrosion resistance, hardness, and wear resistance. To address this limitation and improve corrosion properties, it is preferable to simultaneously deposit a second phase (Algailani et al., 2020; Saravanan et al., 2020; Shahbaznejad & Ebrahimifar, 2021). Oxides of reactive elements, such as ZrO_2, Y_2O_3, and CeO_2, increase the adhesion of the coating to the metal substrate and improve its corrosion resistance (Exbrayat et al., 2017; Shajahan & Basu, 2020; Wang et al., 2017; Wu et al., 2023).

The microstructure and final properties of the coating depend on many parameters. Factors such as the concentration of particles in the plating bath and the pH of the plating solution affect the amount of particles in the coating, morphology, mechanical properties, and corrosion behavior. Other effective parameters in electroless plating include bath temperature, plating time, and the presence of various additives (Deepthi & Krishna, 2018; Mousavi Anijdan et al., 2018; Sarkar et al., 2018; Shozib et al., 2021).

This study aimed to investigate the effect of pH on the microstructure and corrosion behavior of the Ni-Co-La_2O_3-CeO_2 composite coating deposited on AISI 430 stainless steel. A scanning electron microscope (SEM) was used to observe the morphology of the coatings. Potentiodynamic polarization and electrochemical impedance spectroscopy were employed to investigate the corrosion behavior of these coatings. For the first time, this work studied the effect of temperature on the microstructure and corrosion behavior of this iron-based composite coating.

2. MATERIALS AND METHODS

In this study, AISI 430 stainless steel was used as the substrate. Table 1 shows the chemical composition of this steel.

TABLE 1. Chemical composition of AISI 430 steel

Element	P	S	Si	Mn	Cr	C	Fe
wt%	0.03	0.02	0.85	0.92	17.4	0.12	Bal

Pieces of steel with dimensions of 10 mm × 10 mm × 3 mm were cut and then polished with sandpaper grits of 200, 500, 800, 1000, 2000, and 2500. To degrease, the samples were first washed with a soapy water solution and then rinsed with acetone. For surface preparation, each sample was initially placed in a phosphoric acid solution with a current density of 1 $A \cdot cm^{-2}$ for 3 minutes. The samples were then washed with distilled water and activated in a solution of 25% hydrochloric acid and 5% nitric acid for one minute, followed by another wash with distilled water. Each component in the bath plays one or more roles in the plating operation: nickel sulfate supplies nickel ions, cobalt sulfate provides cobalt ions, sodium hypophosphite acts as the reducing agent, sodium citrate serves as the complexing agent, ammonium chloride functions as the buffer, and lanthanum and cerium oxides provide the oxide phase in the plating bath. Table 2 shows the composition of the electroless plating bath. A dilute solution of sodium hydroxide and sulfuric acid was used to adjust the pH before and during the electroless process. After the plating process was completed, the samples were washed with distilled water and dried. To investigate the effect of pH on the microstructure and corrosion behavior of the coating, electroless plating was performed at various pH levels of 8, 8.5, 9, 9.5, and 10.

TABLE 2. Chemical composition of the electroless bath of Ni-Co-La_2O_3-CeO_2 coating

Material	Concentration (g/L)
Cobalt(II) sulfate ($CoSO_4$)	20
Nickel(II) sulfate ($NiSO_4$)	50
Cerium(IV) oxide (CeO_2)	10
Lanthanum oxide (La_2O_3)	10
Sodium hypophosphite ($NaPO_2H_2$)	6
Ammonium chloride (NH_4Cl)	50
Trisodium citrate ($Na_3C_6H_5O_7$)	70

A Cam Scan MV 2300 scanning electron microscope equipped with an EDS analyzer was used to investigate the microstructure of the samples. X-ray diffraction (XRD) was also carried out using a Philips X'Pert High Score diffractometer with Cu Kα radiation (λ = 1.5405 Å) to identify the phases present in the coated samples. Before any electrochemical test (potentiodynamic polarization and electrochemical impedance spectroscopy), each sample was connected to a copper wire and then mounted with epoxy resin. These electrochemical experiments were performed in a distilled water solution containing 3.5% NaCl (Merck) at ambient temperature using an EG&G Princeton Applied Research PARSTAT 2273 potentiostat/galvanostat Model 273A. The samples were immersed in the solution for 60 minutes to achieve a stable state. A commonly used three-electrode setup was employed, consisting of a working electrode (coated or uncoated sample), a saturated calomel electrode (SCE) as the reference electrode, and a platinum rod as the counter electrode (Figure 1). In the potentiodynamic polarization test, polarization was performed from the corrosion potential at a sweep rate of 1 $mV \cdot s^{-1}$ in the anodic and cathodic

directions. Before EIS measurements, all test samples were placed in the test solution for 30 minutes to stabilize. EIS measurements were recorded at the corrosion potential (E_{corr}) and in the frequency range of 10^{-2} to 10^{5} Hz. The AC amplitude used for the experiments was 10 mV. The exposed surface area was 1 cm^2. Princeton Applied Research PowerSuite 2.58 software was used to extract electrochemical data. The extracted potentiodynamic polarization and EIS data were then analyzed using Corrview 3.3 and Zview 3.1 software, respectively.

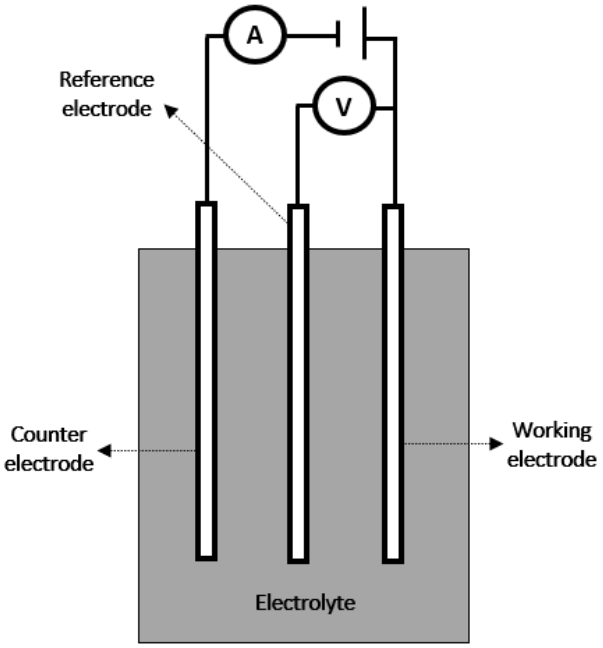

Figure 1. Simple schematic diagram of 3-electrode cell configuration used for the electrochemical investigations

3. RESULTS AND DISCUSSION

To investigate the effect of pH on the morphology and deposition rate of Ni-Co-La_2O_3-CeO_2 coating on AISI 430 stainless steel, coatings were applied at different plating bath pHs of 8, 8.5, 9, 9.5, and 10. Table 3 shows the chemical analysis of these coatings at different pH levels. Figure 2 shows the SEM images of the coatings formed at different pHs at two magnifications (1000x and 2000x).

As shown in Table 3, the amounts of nickel, cobalt, lanthanum oxide, and cerium oxide vary at different pHs. There are no substrate elements at pH = 8, but according to images A1 and A2, which correspond to this pH, oxide particles are dispersed on the surface of the coating. At pH = 8.5, only a small amount of nickel and lanthanum oxide have been deposited on the steel, with the remaining composition being iron. This is consistent with images B1 and B2, which confirm that no coating was formed on the steel surface. As the pH increases to 9, the percentage of coating elements increases, while the percentage of substrate elements decreases. In images C1 and C2, a uniform coating is observed. At pH = 9.5, according to images D1 and D2, a uniform coating has been created, and there is no trace of the substrate in this coating. The amount of lanthanum oxide in this coating is 73.3% by weight, although no cerium oxide was detected. At pH = 10, no coating was formed on the substrate, as indicated by the visible substrate preparation lines in images E1 and E2.

TABLE 3. EDS analysis data for Ni-Co-La_2O_3-CeO_2 coating at different plating bath pHs

	pH=8	pH=8.5	pH=9	pH=9.5	pH=10
Ni (wt%)	63.18	9.23	48.24	58.88	-
Co (wt%)	20.23	-	30.18	28.86	-
La (wt%)	1.48	5.14	8.09	3.73	0.15
Ce (wt%)	1.45	-	2.09	-	-
O (wt%)	4.19	12.39	9.25	6.57	8.82
P (wt%)	1.49	1.15	2.16	1.97	-
Cr (wt%)	-	-	-	-	15.85
Fe (wt%)	-	72.09	-	-	75.17

In the electroless process, H^+ ions are constantly formed, and the pH of the bath must be continuously controlled. There are different theories regarding the effect of pH on the deposition rate of solid particles in the coating. According to Table 3, as the pH of the plating bath increases, the deposition rate of cerium oxide and lanthanum oxide particles first increases and then decreases. With increasing pH, more adsorption sites are occupied by nickel ions, which reduces the adsorption of hydrogen ions on the surface of the particles, thereby increasing the percentage of particles in the coating. Additionally, as pH increases, the roughness of the coating surface increases (Ansari et al., 2017; Imanian Ghazanlou et al., 2018; Julka et al., 2016; Sadeghi & Ebrahimifar, 2021).

Most materials exhibit a zeta potential when placed in an aqueous environment, and this potential is influenced by the pH and ionic strength of the environment. This potential can serve as a criterion for the stability of the suspension. As the pH decreases, ionization causes a reduction in hydroxide ions, making the surface more positive. Conversely, as pH increases, the surface of the particles becomes more negative (Bhattacharjee, 2016). With increasing pH, the zeta potential becomes more negative. In this case, particles with a more negative charge move faster toward the cathode. The repulsive force increases with the rising surface charge of the particles, preventing their agglomeration. Consequently, the stability of the bath improves (Loosli & Stoll, 2017). In the Ni-Co-La_2O_3-CeO_2 coating at pH = 9, both the rate and amount of particle deposition increased. At pH values above 9, the bath became highly unstable, resulting in a decrease in the deposition rate of particles.

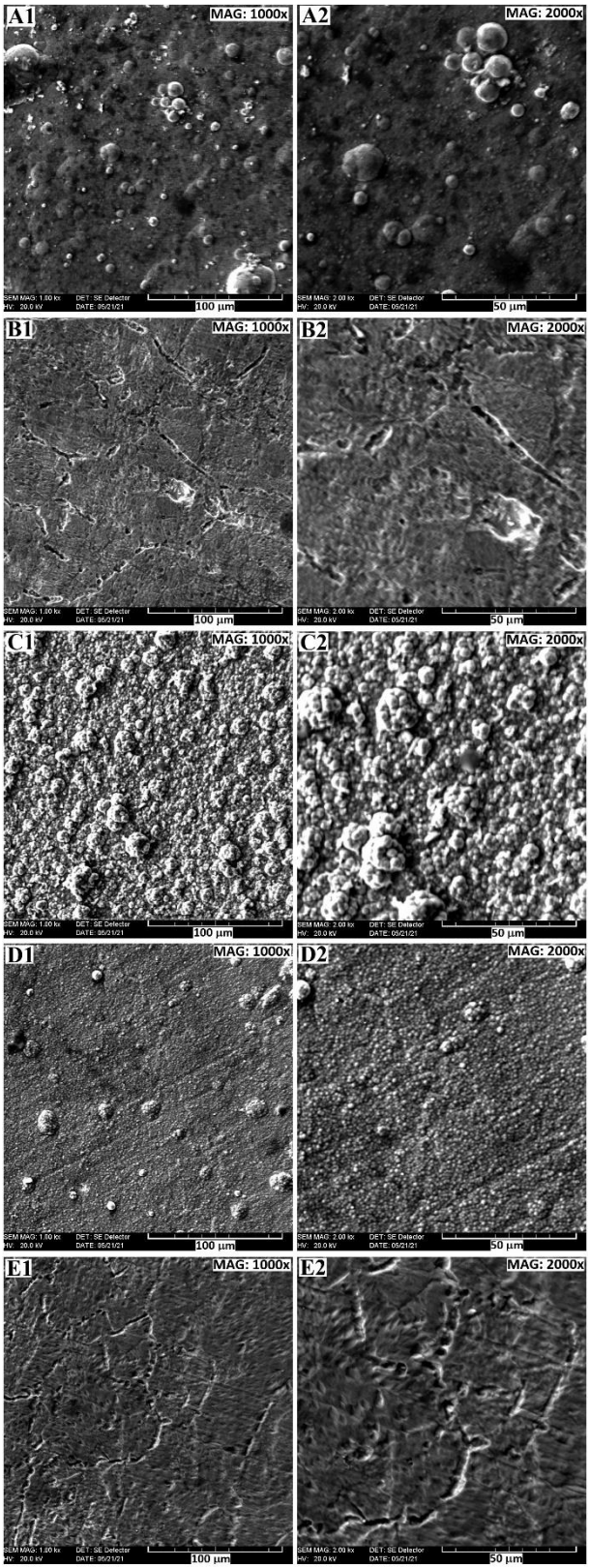

Figure 2. SEM micrographs of the as-coated samples at pH 8 (A1 and A2), pH 8.5 (B1 and B2), pH 9 (C1 and C2), pH 9.5 (D1 and D2), and pH 10 (E1 and E2), respectively.

Figure 3 depicts the results of the XRD analysis of the coated samples. The results revealed that the coatings formed at pH = 8 and pH = 9 consist of phases of cobalt (JCPDS No. 01-1254), nickel (JCPDS No. 04-0850), lanthanum oxide (JCPDS No. 02-0688), and cerium oxide (JCPDS No. 34-0394). The presence of sharper peaks for La_2O_3 and CeO_2 at pH = 9, compared to pH = 8, indicates a higher percentage of these particles in the coating. The presence of substrate peaks (JCPDS No. 87-0721) in the spectrum for coatings formed at pH = 8.5 and pH = 10 indicates the incoherence and non-uniformity of the coatings under these conditions. These results align with the EDS findings.

Figures 4a and 4b show the microscopic image of the cross-sectional view and the corresponding line scan analysis of the Ni-Co-La_2O_3-CeO_2 coating at pH = 9, respectively. The thickness of this monolayer composite coating is approximately 21.7 µm. The line scan analysis confirmed the presence of Ni, Co, and ceramic particles (La_2O_3 and CeO_2) in the coating. The presence of O, La, and Ce throughout the composite coating thickness confirmed the proper distribution of ceramic particles in this coating.

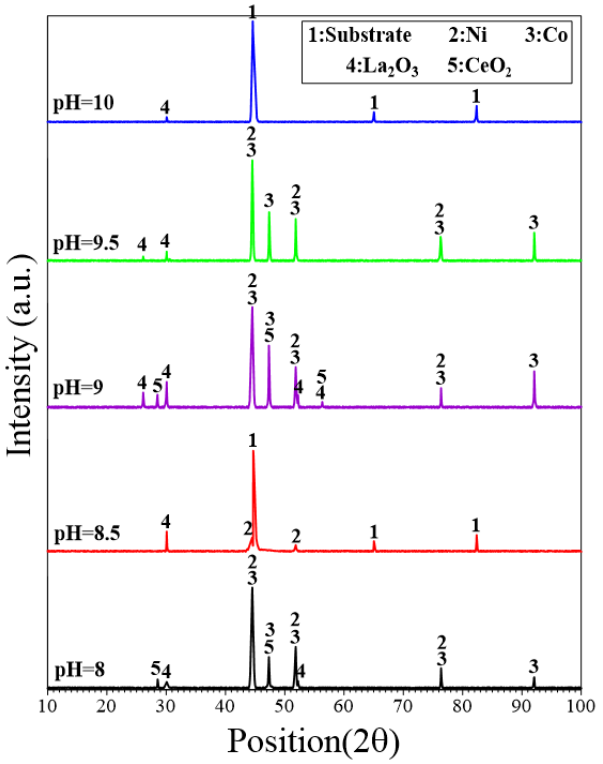

Figure 3. X-ray diffraction patterns of the samples coated at different pHs.

The potentiodynamic polarization curves of the samples coated at different pH values in a 3.5% sodium chloride solution are shown in Figure 5. The data from these curves were analyzed using Corrview software, and the results are presented in Table 4. The Stern-Geary

relationship (Equation 1) was used to calculate the polarization resistance.

$$R_p = \frac{\beta_a \beta_c}{2.303 i_{corr}(\beta_a + \beta_c)} \quad (1)$$

where R_p is the polarization resistance, i_{corr} is the corrosion current density, and β_c and β_a are the slopes of the cathodic and anodic regions of the Tafel curve, respectively (García-Galvan et al., 2021; Goyal et al., 2019; Surani-Yancheshmeh & Ghorbani, 2024). The results indicated that the coating created at pH 9 has the highest polarization resistance (41,064 Ω) and the lowest corrosion current density (0.8 μA·cm^{-2}), resulting in higher corrosion resistance for the coating formed at this pH. With an increase in pH from 9 to 9.5, the polarization resistance decreased sharply, indicating a decrease in corrosion resistance in this case. The significant increase in current density for the coatings formed at pH 8 and pH 10 is due to the lack of formation of a uniform coating on the surface of the substrate.

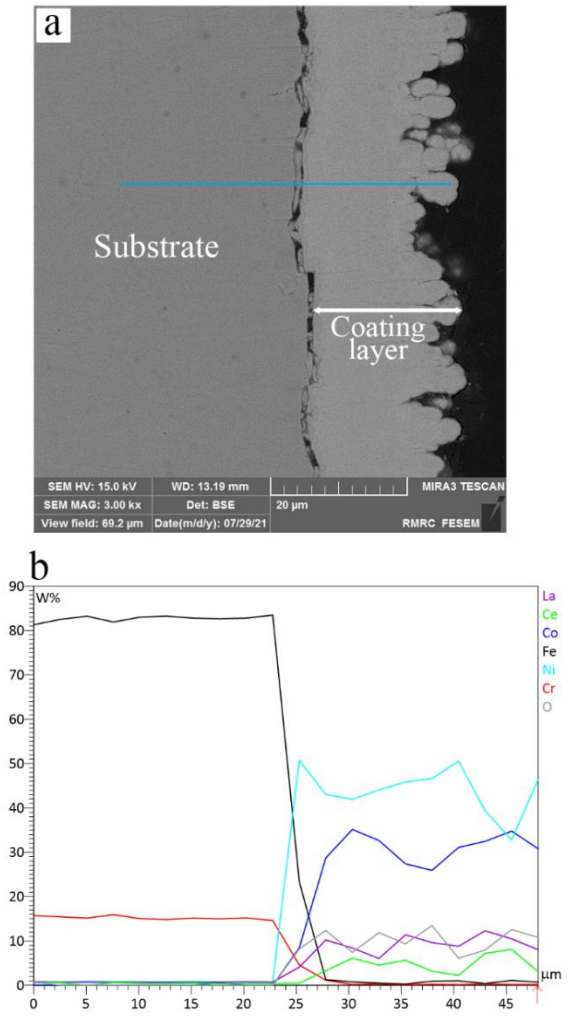

Figure 4. (a) FESEM cross-section micrograph and (b) EDS line scan of the coated sample at pH 9

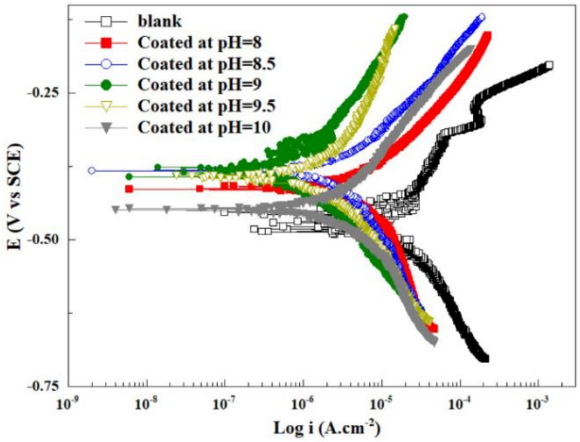

Figure 5. Potentiodynamic polarization curves for Ni-Co-La_2O_3-CeO_2 coating at different pHs

The improvement in the corrosion resistance of the coating deposited at pH 9 can be attributed to the higher concentration of oxide particles (La_2O_3 and CeO_2) present in this coating. In contrast, the corrosion current density for coatings formed at other pH levels is higher due to the lower amount of oxide particles. The uniform distribution of these particles in the coating results in the creation of many galvanic microcells (Shozib et al., 2022). Ceramic particles have higher corrosion resistance and a nobler corrosion potential than the matrix, so these particles act as the cathode while the surrounding matrix serves as the anode. The formation of these galvanic microcells uniformizes the distribution of corrosion current on the coating surface, reducing localized corrosion (Zadeh et al., 2016). Therefore, increasing the concentration and distribution of these particles within the coating shifts the corrosion mechanism from localized corrosion to uniform corrosion (Makarava et al., 2022).

TABLE 4. Electrochemical data derived from potentiodynamic polarization curves of uncoated and coated samples

Sample	blank	Coated at pH=8	Coated at pH=8.5	Coated at pH=9	Coated at pH=9.5	Coated at pH=10
E_{corr} (mV)	-461	-396	-391	-372	-397	-418
i_{corr} (μA.cm^{-2})	17.35	6.05	2.51	0.8	2.04	4.21
β_c (mV.dec^{-1})	229	279.1	165.8	152.2	176.8	265.9
β_a (mV.dec^{-1})	229.3	125.6	132.1	150.4	257.1	175.2
R_p (Ω.cm^2)	2867	6219	12721	41064	22298	10894

The Nyquist curves obtained from electrochemical impedance tests for the uncoated sample and samples coated at pH levels 8, 8.5, 9, 9.5, and 10 are shown in Figure 6. Figures 7a and 7b display the Bode and Bode-

phase diagrams for the tested samples, respectively. As seen, the Bode-phase vs. frequency plots show two distinct peaks for the coated samples. This suggests that the corrosion process of the coated samples can be described by two-time constants, confirmed by the presence of two loops in the Nyquist plots. The first time constant, related to high frequencies, is attributed to the coating/electrolyte interface, while the second, associated with low frequencies, refers to the substrate/electrolyte interface conditions. In contrast, the uncoated sample shows only one-time constant at low frequencies, indicative of the substrate's corrosion process (Kaveh et al., 2023). All EIS curves were plotted in the frequency range of 0.01 Hz to 100 KHz. Data from these diagrams were extracted using Powersuite software and imported into Zview software for analysis. The equivalent circuit proposed by the software for the samples is shown in Figure 8, where R_s represents the solution resistance between the reference electrode and the samples, R_{ct} the charge transfer resistance of the substrate, R_{coat} the resistance of the coating to the penetration of the corrosive environment, and CPE the constant phase element used instead of the simple capacitor. CPE for the double layer and coating are represented as CPE_{dl} and CPE_{coat}, respectively. The constant phase element is used in place of an ideal capacitor to account for the roughness of the electrode surface, heterogeneous reactions, and uneven current distribution during the corrosion process (Xia et al., 2022).

The constant phase element consists of two components: admittance (CPE-T) and power index (CPE-P). The power index ranges between 0.5 and 1, with greater deviation from 1 indicating more inhomogeneity and surface roughness (Dhillon & Kant, 2017; Murariu et al., 2017; Onyeji et al., 2018). The deviation of the Nyquist curve shape from a semicircle indicates surface roughness and non-uniformity during the corrosion process. The results from the EIS curve analysis in Zview software are presented in Table 5. Higher admittance values indicate more porosity in the coating.

Admittance has its lowest value at pH 9, suggesting that the coating's protective properties are best at this pH. As pH increases from 9 to 9.5, admittance values rise, and consequently, corrosion resistance decreases.

The higher solution resistance (25.2 Ω·cm²) at pH 9 could be due to the more effective formation of the composite coating at this pH. Additionally, the double layer capacitance for the coating formed at this pH is lower than in other cases, indicating less corrosive solution penetration to the metal/coating interface (Pajkossy & Jurczakowski, 2017; Ryl et al., 2019; Shanaghi et al., 2023). These results are in complete agreement with the results obtained from Tafel polarization.

One of the most important parameters obtained from the impedance analysis is the charge transfer resistance. This parameter serves as a criterion for the corrosion rate under the coating for the coated samples. An increase in this resistance indicates a decrease in the transfer of aggressive ions through the coating to the surface of the substrate. The value of this parameter is higher for the sample coated at pH = 9 than for the other samples. This can be attributed to the higher percentage of oxide particles in this coating. In fact, the inert properties of these particles increase the charge transfer resistance, and by blocking the charge transfer sites and passivating the surface, they act as a deterrent against aggressive ions. Therefore, these particles force the aggressive ions to move in zigzag paths toward the surface of the substrate, consequently, access to the substrate by the aggressive ions becomes more difficult.

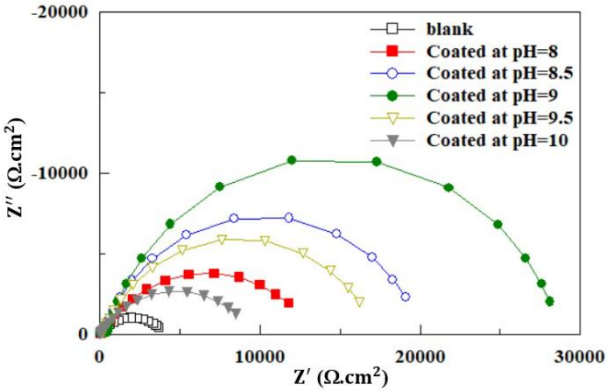

Figure 6. Nyquist curves for Ni-Co-La_2O_3-CeO_2 coating at different pHs

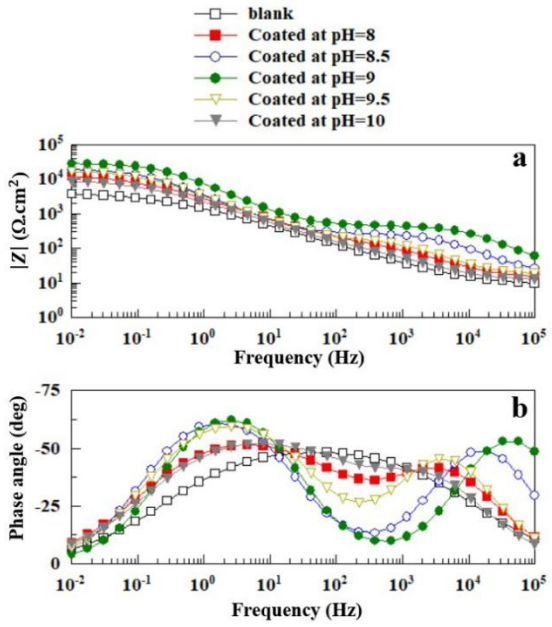

Figure 7. (a) Bode and (b) Bode-phase curves for Ni-Co-La_2O_3-CeO_2 coating at different pHs

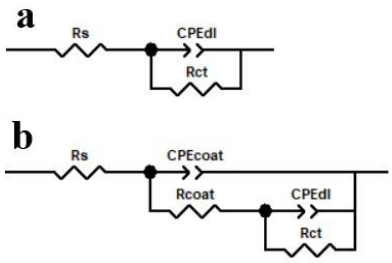

Figure 8. Equivalent electrical circuit used for the (a) uncoated and (b) coated samples

TABLE 5. Electrochemical data derived from impedance curves of uncoated and coated samples

	blank	Coated at pH=8	Coated at pH=8.5	Coated at pH=9	Coated at pH=9.5	Coated at pH=10
R_s ($\Omega.cm^2$)	8.23	14.2	19.4	25.2	17.5	11.7
R_{ct} ($\Omega.cm^2$)	4089	13214	19840	28318	17060	9446
CPE-T_{dl}×10^6 ($\Omega^{-1}.cm^{-2}.S^n$)	190	88.7	62.5	27.4	65.5	98.4
CPE-P_{dl} ($\Omega^{-1}.cm^{-2}.S^n$)	0.58	0.65	0.81	0.84	0.77	0.63
R_{coat} ($\Omega.cm^2$)	-	137	247	429	177	102
CPE-T_{coat}×10^6 ($\Omega^{-1}.cm^{-2}.S^n$)	-	10.2	80.6	0.186	3.62	25.4
CPE-P_{coat} ($\Omega^{-1}.cm^{-2}.S^n$)	-	0.77	0.854	0.87	0.84	0.74

4. CONCLUSION(S)

AISI 430 stainless steel was coated with electroless Ni-Co-La_2O_3-CeO_2 coating. The effect of plating bath pH on the microstructure and corrosion resistance of the formed coatings was investigated. The results showed that the Ni-Co-La_2O_3-CeO_2 deposit obtained in a bath with pH = 9 was uniform. Moreover, the coating formed at this pH had the highest amount of oxide particles compared to the other coatings.

The results of the potentiodynamic polarization test in 3.5 wt% NaCl aqueous solution showed that the sample coated in a bath with pH = 9 had the highest charge transfer resistance (41062 $\Omega.cm^2$) compared to the uncoated (2867 $\Omega.cm^2$), coated samples at pH=8 (6219 $\Omega.cm^2$), pH=8.5 (12721 $\Omega.cm^2$), pH=9.5 (22298 $\Omega.cm^2$) and pH=10 (10894 $\Omega.cm^2$).

ACKNOWLEDGEMENT

The authors would like to acknowledge Shahid Bahonar University of Kerman for all supports throughout this research.

REFRENCES

1. Algailani, H., Mahmoud, A., & Al-Kaisy, H. (2020). Fabrication of Ni-ZrO_2 nanocomposite coating by electroless deposition technique. *Engineering and Technology Journal*, *38*(5). https://doi.org/10.30684/etj.v38i5a.491
2. Amin, M. A., Saracoglu, M., El-Bagoury, N., Sharshar, T., Ibrahim, M. M., Wysocka, J., Krakowiak, S., & Ryl, J. (2016). Microstructure and corrosion behaviour of carbon steel and ferritic and austenitic stainless steels in NaCl solutions and the effect of p-nitrophenyl phosphate disodium salt. *International Journal of Electrochemical Science*, *11*(12). https://doi.org/10.20964/2016.12.17
3. Ansari, M. I., Julka, S., & Thakur, D. G. (2017). Enhancement of surface properties with influence of bath pH on electroless Ni-P-ZnO/Al_2O_3 nano-composite deposits for defence applications. *Journal of Molecular Liquids*, *247*. https://doi.org/10.1016/j.molliq.2017.09.030
4. Bhattacharjee, S. (2016). DLS and zeta potential - What they are and what they are not? In *Journal of Controlled Release*. 235. https://doi.org/10.1016/j.jconrel.2016.06.017
5. Chen, K., Wang, J., Zhang, L., Wang, H., An, X., Li, Y., Zhang, J., Shen, Z., & Zeng, X. (2022). A high-resolution study of the different surface state effects on the corrosion behaviors of a ferritic steel and an austenitic steel in supercritical water. *Corrosion Science*, *209*. https://doi.org/10.1016/j.corsci.2022.110757
6. Chintada, V. B., Koona, R., & Raju Bahubalendruni, M. V. A. (2021). State of art review on nickel-based electroless coatings and materials. In *Journal of Bio- and Tribo-Corrosion*. *7(4)*. https://doi.org/10.1007/s40735-021-00568-7
7. Deepthi, Y. P., & Krishna, M. (2018). Optimization of electroless copper coating parameters on graphite particles using taguchi and grey relational analysis. *Materials Today: Proceedings*, *5(5)*. https://doi.org/10.1016/j.matpr.2018.02.183
8. Dhillon, S., & Kant, R. (2017). Theory for electrochemical impedance spectroscopy of heterogeneous electrode with distributed capacitance and charge transfer resistance. *Journal of Chemical Sciences*, *129*(8). https://doi.org/10.1007/s12039-017-1335-x
9. Elkhoshkhany, N., Hafnway, A., & Khaled, A. (2017). Electrodeposition and corrosion behavior of nano-structured Ni-WC and Ni-Co-WC composite coating. *Journal of Alloys and Compounds*, *695*. https://doi.org/10.1016/j.jallcom.2016.10.290
10. Exbrayat, L., Rébéré, C., Ndong Eyame, R., Steyer, P., & Creus, J. (2017). Corrosion behaviour in saline solution of pulsed-electrodeposited zinc-nickel-ceria nanocomposite coatings. *Materials and Corrosion*, *68*(10). https://doi.org/10.1002/maco.201709419
11. Fayomi, O. S. I., Akande, I. G., & Sode, A. A. (2019). Corrosion prevention of metals via electroless nickel coating: A review. *Journal of Physics: Conference Series*, *1378*(2). https://doi.org/10.1088/1742-6596/1378/2/022063
12. García-Galvan, F. R., Fajardo, S., Barranco, V., & Feliu, S. (2021). Experimental apparent stern–geary coefficients for AZ31B Mg alloy in physiological body fluids for accurate corrosion rate determination. *Metals*, *11*(3). https://doi.org/10.3390/met11030391
13. Goyal, A., Pouya, H. S., Ganjian, E., Olubanwo, A. O., & Khorami, M. (2019). Predicting the corrosion rate of steel in cathodically protected concrete using potential shift. *Construction and Building Materials*, *194*. https://doi.org/10.1016/j.conbuildmat.2018.10.153
14. Imanian Ghazanlou, S., Farhood, A. H. S., Hosouli, S., Ahmadiyeh, S., & Rasooli, A. (2018). Pulse and direct electrodeposition of Ni–Co/micro and nanosized SiO_2 particles. *Materials and Manufacturing Processes*, *33*(10). https://doi.org/10.1080/10426914.2017.1364748

15. Julka, S., Ansari, M. I., & Thakur, D. G. (2016). Effect of pH on mechanical, physical and tribological properties of electroless Ni-P-Al_2O_3 composite deposits for marine applications. *Journal of Marine Science and Application*, *15*(4). https://doi.org/10.1007/s11804-016-1385-3

16. Kaveh, M., Sajjadnejad, M., Mohassel, A., & Setoudeh, N. (2023). Influence of B_4C nanoparticles on corrosion characteristics of Ni matrix nanocomposite coatings fabricated via pulse electroplating technique. *Advanced Ceramics Progress*, *9(3)*, 16-30. https://doi.org/10.30501/acp.2024.429141.1141

17. Kumar, S., Banerjee, T., & Patel, D. (2020). Tribological characteristics of electroless multilayer coating: A review. *Materials Today: Proceedings*, *33*. https://doi.org/10.1016/j.matpr.2020.04.207

18. Loosli, F., & Stoll, S. (2017). Effect of surfactants, pH and water hardness on the surface properties and agglomeration behavior of engineered TiO_2 nanoparticles. *Environmental Science: Nano*, *4*(1). https://doi.org/10.1039/c6en00339g

19. Makarava, I., Esmaeili, M., Kharytonau, D. S., Pelcastre, L., Ryl, J., Bilesan, M. R., Vuorinen, E., & Repo, E. (2022). Influence of CeO_2 and TiO_2 particles on physicochemical properties of composite nickel coatings electrodeposited at ambient temperature. *Materials*, *15*(16). https://doi.org/10.3390/ma15165550

20. Mosavi, A., & Ebrahimifar, H. (2020). Investigation of oxidation and electrical behavior of AISI 430 steel coated with Mn–Co–CeO_2 composite. *International Journal of Hydrogen Energy*, *45*(4). https://doi.org/10.1016/j.ijhydene.2019.11.183

21. Mousavi Anijdan, S. H., Sabzi, M., Zadeh, M. R., & Farzam, M. (2018). The effect of electroless bath parameters and heat treatment on the properties of Ni-P and Ni-P-Cu composite coatings. *Materials Research*, *21*(2). https://doi.org/10.1590/1980-5373-MR-2017-0973

22. Murariu, A. C., Pleșu, N., Perianu, I. A., & Tară-Lungă-Mihali, M. (2017). Investigations on corrosion behaviour of WC-CrC-Ni coatings deposited by HVOF thermal spraying process. *International Journal of Electrochemical Science*, *12*(2). https://doi.org/10.20964/2017.02.60

23. Onyeji, L., Mohammed, S., & Kale, G. (2018). Electrochemical response of micro-alloyed steel under potentiostatic polarization in CO_2 saturated brine. *Corrosion Science*, *138*. https://doi.org/10.1016/j.corsci.2018.04.001

24. Pajkossy, T., & Jurczakowski, R. (2017). Electrochemical impedance spectroscopy in interfacial studies. In *Current Opinion in Electrochemistry*. *1(1).* https://doi.org/10.1016/j.coelec.2017.01.006

25. Pancrecious, J. K., Ulaeto, S. B., Ramya, R., Rajan, T. P. D., & Pai, B. C. (2018). Metallic composite coatings by electroless technique–a critical review. In *International Materials Reviews*. *63(8).* https://doi.org/10.1080/09506608.2018.1506692

26. Ryl, J., Burczyk, L., Zielinski, A., Ficek, M., Franczak, A., Bogdanowicz, R., & Darowicki, K. (2019). Heterogeneous oxidation of highly boron-doped diamond electrodes and its influence on the surface distribution of electrochemical activity. *Electrochimica Acta*, *297*. https://doi.org/10.1016/j.electacta.2018.12.050

27. Sadeghi, S., & Ebrahimifar, H. (2021). Effect of electrolyte pH on microstructure, corrosion behavior, and mechanical behavior of Ni-P-W-TiO_2 electroplated coatings. *Journal of Materials Engineering and Performance*, 30(4). https://doi.org/10.1007/s11665-021-05462-4

28. Saravanan, I., Elayaperumal, A., Devaraju, A., Karthikeyan, M., & Raji, A. (2020). Wear behaviour of electroless Ni-P and Ni-P-TiO_2 composite coatings on En8 steel. *Materials Today: Proceedings*, *22*. https://doi.org/10.1016/j.matpr.2019.12.007

29. Sarkar, S., Baranwal, R. K., Banerjee, S., Prakash, A., Mandal, R., & Majumdar, G. (2018). Parametric optimization of process parameters on the response of microhardness of electroless Ni-P coating. *Journal of Molecular and Engineering Materials*, *06*(01n02). https://doi.org/10.1142/s225123731850003x

30. Shahbaznejad, H., & Ebrahimifar, H. (2021). A study on the oxidation and electrical behavior of crofer 22 APU solid oxide fuel cell interconnects with Ni-Co-CeO_2 composite coating. *Journal of Materials Science: Materials in Electronics*, 32(6). https://doi.org/10.1007/s10854-021-05470-z

31. Shajahan, S., & Basu, A. (2020). Corrosion, oxidation and wear study of electro-co-deposited ZrO_2-TiO_2 reinforced Ni-W coatings. *Surface and Coatings Technology*, *393*. https://doi.org/10.1016/j.surfcoat.2020.125729

32. Shanaghi, A., Souri, A. R., & Forghani, W. (2023). Comparative study of anodized titanium surfaces: The effect of low voltage on the morphology, performance, and corrosion resistance of the double layer. *Advanced Ceramics Progress*, 9(2), 1-7. https://doi.org/10.30501/acp.2023.383589.1116

33. Shozib, I. A., Ahmad, A., Abdul-Rani, A. M., Beheshti, M., & Aliyu, A. A. (2022). A review on the corrosion resistance of electroless Ni-P based composite coatings and electrochemical corrosion testing methods. In *Corrosion Reviews* (Vol. 40, Issue 1). https://doi.org/10.1515/corrrev-2020-0091

34. Shozib, I. A., Ahmad, A., Rahaman, M. S. A., Abdul-Rani, A. M., Alam, M. A., Beheshti, M., & Taufiqurrahman, I. (2021). Modelling and optimization of microhardness of electroless Ni-P-TiO_2 composite coating based on machine learning approaches and RSM. *Journal of Materials Research and Technology*, *12*. https://doi.org/10.1016/j.jmrt.2021.03.063

35. Surani-Yancheshmeh, H., & Ghorbani, M. (2024). Corrosion studies on pulse reverse Ni–Mo coatings electrodeposited on Cu substrate. *Electrochimica Acta*, *478*. https://doi.org/10.1016/j.electacta.2024.143828

36. Wang, L., Chen, M., Liu, H., Jiang, C., Ji, V., & Moreira, F. (2017). Optimisation of microstructure and corrosion resistance of Ni-Ti composite coatings by the addition of CeO_2 nanoparticles. *Surface and Coatings Technology*, *331*. https://doi.org/10.1016/j.surfcoat.2017.10.049

37. Wu, T., Ma, M., Ding, K., Nan, X., Wang, Z., Wei, X., & Zhu, X. (2023). Effect of Y_2O_3 nanoparticles on the microstructure and corrosion resistance of electrodeposited Ni-Mo-Y_2O_3 nanocomposite coatings. *International Journal of Electrochemical Science*, 18(6). https://doi.org/10.1016/J.IJOES.2023.100095

38. Xia, D. H., Deng, C. M., Macdonald, D., Jamali, S., Mills, D., Luo, J. L., Strebl, M. G., Amiri, M., Jin, W., Song, S., & Hu, W. (2022). Electrochemical measurements used for assessment of corrosion and protection of metallic materials in the field: A critical review. In *Journal of Materials Science and Technology 112*. https://doi.org/10.1016/j.jmst.2021.11.004

39. Yu, Y., Shironita, S., Souma, K., & Umeda, M. (2018). Effect of chromium content on the corrosion resistance of ferritic stainless steels in sulfuric acid solution. *Heliyon*, 4(11). https://doi.org/10.1016/j.heliyon.2018.e00958

40. Zadeh, K. M., Shakoor, R. A., & Bahgat Radwan, A. (2016). Structural and electrochemical properties of electrodeposited Ni-P nanocomposite coatings containing mixed ceramic oxide particles. *International Journal of Electrochemical Science*, *11*(8). https://doi.org/10.20964/2016.08.42